

Ellipsoidal plasma mirror focusing of high power laser pulses to ultra-high intensities

R. Wilson, M. King, R. J. Gray, D. C. Carroll, R. J. Dance, C. Armstrong, S. J. Hawkes, R. J. Clarke, D. J. Robertson, D. Neely, and P. McKenna

Citation: *Physics of Plasmas* **23**, 033106 (2016); doi: 10.1063/1.4943200

View online: <http://dx.doi.org/10.1063/1.4943200>

View Table of Contents: <http://scitation.aip.org/content/aip/journal/pop/23/3?ver=pdfcov>

Published by the *AIP Publishing*

Articles you may be interested in

[High efficiency proton beam generation through target thickness control in femtosecond laser-plasma interactions](#)

Appl. Phys. Lett. **104**, 214101 (2014); 10.1063/1.4879641

[Relativistic self-focusing of ultra-high intensity X-ray laser beams in warm quantum plasma with upward density profile](#)

Phys. Plasmas **21**, 052705 (2014); 10.1063/1.4876751

[Electron heating mode transition induced by ultra-high frequency in atmospheric microplasmas for biomedical applications](#)

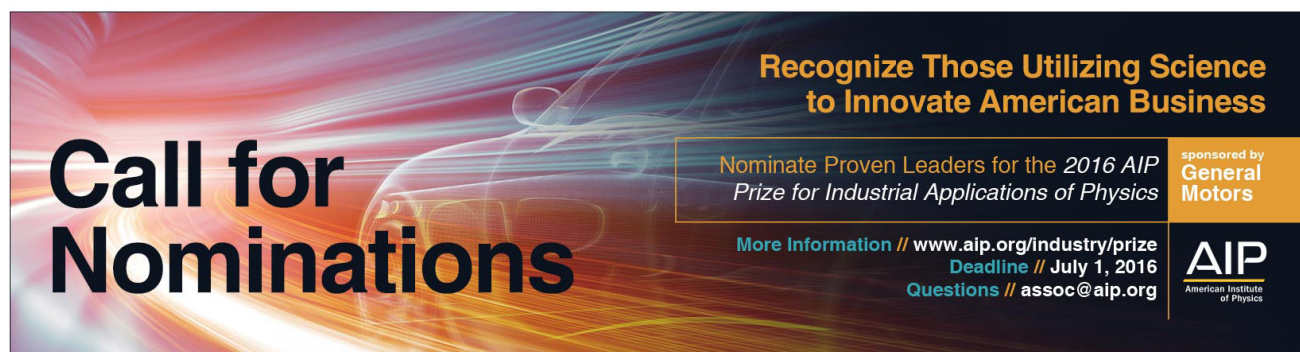
Appl. Phys. Lett. **100**, 183702 (2012); 10.1063/1.4711207

[Femtosecond laser induced plasma diffraction gratings in air as photonic devices for high intensity laser applications](#)

Appl. Phys. Lett. **94**, 251104 (2009); 10.1063/1.3157908

[Particle-in-cell simulations of ultra intense laser pulses propagating through overdense plasma for fast-ignitor and radiography applications](#)

Phys. Plasmas **6**, 2041 (1999); 10.1063/1.873496



Call for Nominations

Recognize Those Utilizing Science to Innovate American Business

Nominate Proven Leaders for the 2016 AIP Prize for Industrial Applications of Physics

More Information // www.aip.org/industry/prize
Deadline // July 1, 2016
Questions // assoc@aip.org

sponsored by General Motors

AIP
American Institute of Physics

Ellipsoidal plasma mirror focusing of high power laser pulses to ultra-high intensities

R. Wilson,¹ M. King,¹ R. J. Gray,¹ D. C. Carroll,² R. J. Dance,¹ C. Armstrong,^{1,2}
 S. J. Hawkes,² R. J. Clarke,² D. J. Robertson,³ D. Neely,^{2,1} and P. McKenna^{1,a)}

¹*SUPA Department of Physics, University of Strathclyde, Glasgow G4 0NG, United Kingdom*

²*Central Laser Facility, STFC Rutherford Appleton Laboratory, Oxfordshire OX11 0QX, United Kingdom*

³*Department of Physics, Durham University, South Road, Durham DH1 3LE, United Kingdom*

(Received 25 January 2016; accepted 22 February 2016; published online 7 March 2016)

The design and development of an ellipsoidal F/1 focusing plasma mirror capable of increasing the peak intensity achievable on petawatt level laser systems to $>10^{22} \text{ W cm}^{-2}$ is presented. A factor of 2.5 reduction in the focal spot size is achieved when compared to F/3 focusing with a conventional (solid state) optic. We find a factor of 3.6 enhancement in peak intensity, taking into account changes in plasma mirror reflectivity and focal spot quality. The sensitivity of the focusing plasma optic to misalignment is also investigated. It is demonstrated that an increase in the peak laser intensity from $3 \times 10^{20} \text{ W cm}^{-2}$ to $10^{21} \text{ W cm}^{-2}$ results in a factor of 2 increase in the maximum energy of sheath-accelerated protons from a thin foil positioned at the focus of the intense laser light. © 2016 AIP Publishing LLC. [<http://dx.doi.org/10.1063/1.4943200>]

INTRODUCTION

Throughout the history of high-power laser-plasma science, new avenues of research have been enabled by increasing the peak laser intensity achievable. These include laser-driven particle acceleration,^{1,2} radiation sources,^{3,4} relativistic optics,^{5,6} laboratory astrophysics,^{7,8} and warm dense matter.^{9,10} Peak intensities in the range of $10^{20} - 10^{21} \text{ W cm}^{-2}$ are now available at hundred-terawatt-to-petawatt-scale laser facilities. In a few years, multi-petawatt laser systems such as APOLLON¹¹ and the extreme light infrastructure (ELI)¹² facilities will start operation. These lasers are expected to achieve focused intensities in the range of $10^{22} - 10^{23} \text{ W cm}^{-2}$, which will enable the exploration of ultra-intense laser-plasma phenomena, such as high-field quantum electrodynamics (QED).^{13,14}

The typical approach adopted to increasing the peak intensity involves increasing the laser pulse energy or decreasing its duration. When using conventional solid state optics, these approaches typically require an increase in the beam diameter to keep the energy density on the optic below the damage threshold. Alternatively, the focal spot size can be decreased, by implementing a small F-number (F/#) focusing optic (large numerical aperture). Such optics are typically expensive and are susceptible to damage from target debris due to their short focal length (and thus close proximity to the target).

The development of single-use, disposable plasma-based optics enables many of these short-comings to be avoided. Crucially, plasma mirrors operate at a much higher energy density and are therefore more than an order of magnitude smaller than conventional solid state optics, and can thus be manufactured at much lower cost. Their disposable nature means that target debris is not an issue. Planar plasma mirrors (PPMs)^{15,16} are now routinely used at many high power laser

facilities as a valuable tool for suppressing laser pre-pulses and amplified spontaneous emission (ASE) inherently present in intense laser pulses produced via the chirped pulse amplification (CPA) process.¹⁷ The basic principle of the plasma mirror is that a thin plasma is created on the surface of a solid which is otherwise transparent to the laser light (typically anti-reflection (AR) coated, optical quality glass). Laser light is reflected at the critical density—the electron density at which the plasma electron oscillation frequency is equal to the laser frequency. The laser intensity on the surface is chosen such that undesired pre-pulses and ASE light preceding the main pulse are below the threshold intensity required to ionise the medium and are therefore transmitted through it. In this way, the main pulse which is reflected from the plasma has a sharper rising edge and higher intensity contrast (ratio of the peak intensity to the intensity of the ASE pedestal). PPMs have been used in this way to enable experimentation with ultra-thin target foils, resulting in the development of new ion acceleration¹⁸ and high-harmonic generation^{19,20} mechanisms. In addition, there have been several dedicated studies undertaken to understand and characterise these important optical components.^{21–24}

The fact that light is reflected from a thin plasma layer formed on the substrate surface means that the surface can be curved to induce focusing (just as in conventional solid state optics). By appropriate choice of the surface curvature, an incident focusing laser beam can be made to focus with an even smaller F/#. A focusing plasma mirror (FPM) of ellipsoidal geometry with two foci, such that demagnification of a focal spot occurs from one focal position to the other, satisfies the need to have off-axis focusing to ensure that the target is not blocking the incoming laser beam. Such an optic is attractive not only because of the increase in peak laser intensity achievable but also because it improves pulse intensity contrast in the same way as a PPM. The use of such an optic was first demonstrated in a proof-of-principle

^{a)}Electronic mail: paul.mckenna@strath.ac.uk

experiment on a terawatt (TW) level laser system reported by Kon *et al.*²⁵ and Nakatsutsumi *et al.*,²⁶ whereby an F/0.4 FPM was developed and achieved a five-fold reduction in focal spot size compared to the spot formed by a conventional F/2.7 off-axis parabolic (OAP) mirror. The intensity enhancement was indirectly diagnosed by the measurement of the maximum energy of protons accelerated from a thin target foil positioned at the FPM beam focus.

In this article, we report on the design, development, and testing of an ellipsoidal FPM to be utilised on a petawatt (PW) scale laser system; the Vulcan petawatt laser at the Rutherford Appleton Laboratory in the UK. The overall performance of the optic, including its sensitivity to optical misalignment, is investigated experimentally. The use of the FPM to enhance the maximum energy of sheath-accelerated protons is demonstrated.

PRINCIPLES OF DESIGN AND OPERATION

As in the case of the previously trialled FPM,^{25,26} an ellipsoidal geometry was chosen to induce the plasma mirror focusing, as depicted in Fig. 1(b). This shape has two foci positions, f_1 and f_2 , located along the major axis, equidistant from the centre. This enables point-to-point (i.e., focus-to-focus) imaging. Depending on the degree of elliptical eccentricity, e , a reduction or enlargement in the image size at one focus can be obtained when an object is placed at the other, i.e., the magnification of the optic. The magnification is equal to the ratio of lengths β/α , where α is defined as the distance from f_1 to a point on the mirror surface and β is defined as the distance from the same point to f_2 . The ratio changes as a function of the beam incident angle, θ_{in} , with respect to the major axis and can therefore be expressed as²⁷

$$m = \frac{(1 + e^2) - 2e \cdot \cos \theta_{in}}{(1 - e^2)}, \quad (1)$$

where the eccentricity is given by $e = \sqrt{(1 - b^2/a^2)}$; a and b being the semi-major and semi-minor axis length, respectively.

In practical terms, a conventional OAP can be aligned such that the focus coincides with f_1 of the FPM. As the light diverges beyond f_1 , it reflects from the plasma it forms on the curved optic surface and is imaged to position f_2 . The focal spot at f_1 is demagnified at f_2 depending on the chosen geometry of the FPM and the angle θ_{in} .

OPTIC DESIGN

The precise design of a FPM depends on the pulse parameters of the laser system on which it is intended to be used. It depends chiefly on the laser pulse peak power and the F/# of the conventional OAP used to bring the beam to position f_1 . The optic developed in this study has been designed for use on the Vulcan PW laser at Rutherford Appleton Laboratory. This laser delivers pulses of 1053 nm light, with energy 500–600 J pre-compressor (typically ~ 200 J on-target including losses in the compressor and plasma mirror), and duration ~ 750 fs (FWHM). The pulse is focused using an F/3.1 OAP to produce a focal spot of typical diameter of $\sim 4 \mu\text{m}$ (FWHM). The resulting calculated peak intensity is of the order of $6 \times 10^{20} \text{ W cm}^{-2}$ (assuming 30% of the energy is contained within the FWHM focal spot).

As the purpose of the FPM is to increase the achievable peak intensity through focal spot size reduction, the first step in the design is the selection of a suitable demagnification. Although the smallest F/# possible is desired, the smaller the F/# is the more sensitive the FPM becomes to alignment. Thus a compromise value is selected which produces significant intensity enhancement while enabling the ease of use and robustness to a non-optimum beam profile. A value of $\times 3$ demagnification ($m = 1/3$) was selected based on the F/3.1 OAP, such that the FPM is designed to yield a focal spot size of $\sim 1.3 \mu\text{m}$ FWHM (close to the diffraction limit).

The dimensions of the FPM depend on the desired energy reflectivity of the optic and thus the incident laser intensity on the optic surface (the reflectivity dependence on laser intensity is discussed in Refs. 22 and 24). A region of high specular reflectivity ($\sim 70\%$) is established at an

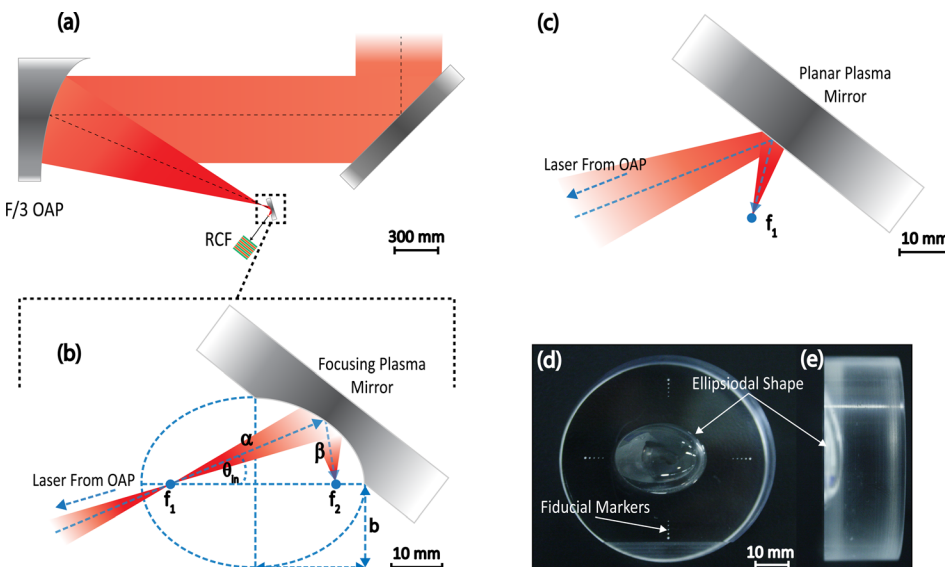


FIG. 1. Schematic diagrams showing: (a) the overall optical set-up in the Vulcan target chamber; (b) the operation of the ellipsoidal focusing plasma mirror, where the incoming laser is focused by a conventional OAP to position f_1 and the FPM focuses the beam to position f_2 , with magnification given by β/α ; (c) the operation of a reference planar plasma mirror. (d) and (e) Photographs of the manufactured FPM optic showing: (d) the front surface and (e) a side view, demonstrating the ellipsoidal structure. The fiducial markers highlighted are used for alignment of the optic.

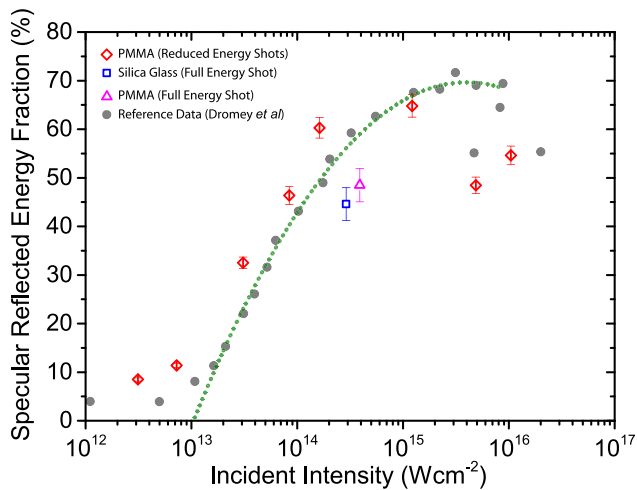


FIG. 2. Percentage of laser light specularly reflected from the plasma mirror surface as a function of the laser intensity at the plasma mirror surface. Red data points are the results from reduced energy Vulcan PW pulses on a flat PMMA sample and the grey points correspond to reference data from Dromey *et al.*²² for a 500fs pulse and a fused silica PPM, with 6° laser incidence angle. A quadratic fit is made to this data between the incident intensities of $10^{13} - 10^{16} \text{ W cm}^{-2}$, as illustrated by the dotted green curve. The blue and purple data points represent full energy shots on flat samples of silica glass and PMMA, respectively. Each data point represents a single laser shot.

incident intensity of $\sim 10^{15} \text{ W cm}^{-2}$, as shown in Fig. 2. The laser intensity at the optic surface is determined by the distance the beam expands from f_1 to the surface, i.e., α in Fig. 1(b). Through consideration of Gaussian beam expansion, this distance can be determined such that an intensity of $10^{15} \text{ W cm}^{-2}$ is achieved, resulting in a high optical reflectivity. For alignment purposes, the incidence angle θ_{in} is selected to be 19.4° for this optimal intensity, along with a selected minimum distance of the focus f_2 from the ellipsoidal surface for practical target placement. Using these parameters, the remaining values required to define the shape of the optic are obtained using simple trigonometric expressions describing an ellipse.

To validate the design before manufacture, analytical modelling was conducted using optical ray-tracing software (Zemax). Figures 3(a) and 3(b) show the results for the input focal spot and the resultant output focus formed by the FPM. This produces a demagnification of $\times 2.9$, based on the input and output focal spots of $1.71 \mu\text{m}$ and $0.59 \mu\text{m}$ (FWHM), respectively. This modelling was conducted using 532 nm light to enable direct comparison with experimental tests discussed in the “Optic Testing” section.

The FPM design (Figs. 1(d) and 1(e)) was manufactured by diamond machining of the ellipsoidal shape into a 20 mm thick cylindrical sample of transparent Poly(methyl methacrylate) (PMMA) plastic. The thickness of the optic was chosen to provide sufficient rigidity to minimise surface distortions that could be induced via mounting. Current optical manufacturing processes, such as this, are capable of optic production with a shape profile error $< 0.1 \mu\text{m}$. Conventional PPMs typically include an AR coating, with reflectivity $\sim 0.3\%$,²⁸ to increase their intensity contrast improvement ability (the achievable contrast enhancement factor is equal to the ratio of the plasma reflectivity to the “cold” reflectivity of the optic²⁹).

The FPMs developed in this study do not include an AR coating at the time of testing, thus characterising their cold reflectivity is important to gauge how they will perform as plasma mirrors. A spectrophotometer was used to measure the reflectivity of 1053 nm p-polarised light from the FPM over a range of incident angles, from 25° to 45° to encompass the full range of illumination angles of the diverging laser beam in the optic design. The average reflectivity was measured to be $(4.2 \pm 0.3)\%$, and thus for the predicted plasma reflectivity of $\sim 70\%$ the optic is expected to increase the intensity contrast by a factor of 16.7, approximately an order of magnitude less than an AR coated plasma mirror.

REFLECTIVITY TESTING

To characterise the plasma reflectivity of the selected FPM substrate material, the Vulcan PW laser was used to investigate the reflectivity of a PPM, made from the same transparent PMMA material, as a function of incident laser intensity. The sample was irradiated with p-polarized pulses, at a 35° incident angle relative to the mirror surface (the same as the operational incident angle of the FPM design). The laser intensity was varied by changing the distance between the optic surface and the laser focus, at which a maximum intensity of approximately $\sim 10^{16} \text{ W cm}^{-2}$ is achieved using $\sim 0.25 \text{ J}$ pulses. The energy of the incident and reflected light was measured using a Gentec pyroelectric energy meter for absolute calorimetry. The specular reflectivity as a function of incident laser intensity is shown in Fig. 2.

A peak specular reflectivity of $(65 \pm 2)\%$ was measured at an intensity of $(1.2 \pm 0.3) \times 10^{15} \text{ W cm}^{-2}$. The overall trend of the reflectivity-intensity dependency is in good agreement with the data used to design the FPM, indicating there is little difference in terms of performance between a typically used substrate material (silica glass) and the plastic material chosen for the FPM design. However, the reflectivity is found to be slightly lower at intensities in the range of $10^{14} - 10^{16} \text{ W cm}^{-2}$ on the two full laser energy shots conducted; from 46%–68% in the reference data to 45%–55% in the experimental shots. This may occur due to the difference in laser incidence angle in the data sets. The results from Dromey *et al.*²² were taken using a low incidence angle (6°) which would result in a reduced laser absorption when compared to the larger incident angle (35°) used in the present investigation. The reduced reflectivity for larger incidence angles has been observed in previous studies, which conclude that this arises due to the increased absorption.^{21,30}

OPTIC TESTING

An experimental set-up utilising a low-power continuous wave (CW) laser was developed to characterise the manufactured FPM design. This enabled the focal spot reduction to be quantified and the feasibility of the use of each optic for laser-target interaction studies to be tested. The set-up was not only used for the focal spot characterisation but also used to pre-align the optics prior to use on the Vulcan PW laser system. In this low-power illumination mode, the

substrate is not ionised and thus the optic simply functions as a conventional partially reflecting solid-state optic.

To emulate the Vulcan PW F/3.1 input focusing beam, an OAP ($f = 145$ mm) and a 48 mm diameter collimated input beam was selected. A 532 nm wavelength laser diode was used as the light source and was propagated through a spatial filter prior to focusing to improve the spatial-intensity profile of the beam. This wavelength of light was utilised for optic testing as it is much lower than the normal operational wavelength (1053 nm), and thus will aid in determining if there are any unwanted irregularities in the optic's focusing, which are displayed more prominently with lower wavelengths. To measure the focal spot formed by both the OAP and FPM, an infinity-corrected microscope objective ($\times 50$ and N.A. = 0.42) was used to image the spot to a CCD camera. For alignment and imaging purposes, both the optic and camera set-up were mounted on micrometer controlled xyz -translation stages, where the z -axis of the FPM motion was set along the direction of the OAP input beam.

Optimum alignment

Characterisation of the optic was conducted by analysing the output focal spot formed by the FPM under optimum alignment, occurring when the OAP input focus spatially coincides with the FPM focus, f_1 . An example result of these is displayed in Figs. 3(c) and 3(d).

The optic testing established that the typical output focal spot formed by the FPM (at f_2), displayed in Fig. 3(d), is $0.76 \mu\text{m}$ (FWHM), with 28.3% energy encircled within the FWHM diameter. As the input focal spot, shown in Fig. 3(c), was $1.91 \mu\text{m}$ (FWHM) with 35.1% FWHM encircled energy, a focal spot demagnification of $\times 2.51$ is achieved. The reduction in encircled energy may be attributed to small optic misalignments or inherent deviations in the optics shape from optimal design. It should be noted that this encircled energy is larger than the FPM fielded in the first proof-of-principle experiment²⁶ for which 17% is reported. Both experiment and ray-tracing results are in good agreement with the theoretically predicted demagnification of $\times 3$ for the design.

Using the above characterisation results, the expected enhancement factor in the laser intensity, I_{Enh} , under plasma operation can be calculated. This parameter depends on the input (ϕ_{in}) and output (ϕ_{out}) spot sizes, the FWHM encircled energies (E_{in} and E_{out} , respectively), and the plasma optic reflectivity (Γ_p) as follows:

$$I_{Enh} = (\phi_{in}/\phi_{out})^2 \cdot \Gamma_p \cdot (E_{out}/E_{in}). \quad (2)$$

For a plasma reflectivity equal to 70%, the intensity enhancement implied from testing, in Figs. 3(c) and 3(d), is $\times 3.6$. The minimum reflectivity at which enhancement can be achieved is 19.7%.

The focal spot expected to be achieved with the FPM was also characterised using the Vulcan PW laser, again far below the ionisation threshold. Figures 3(e) and 3(f) display the typical input and output focal spot images produced. This differs from the testing set-up in which this system has a

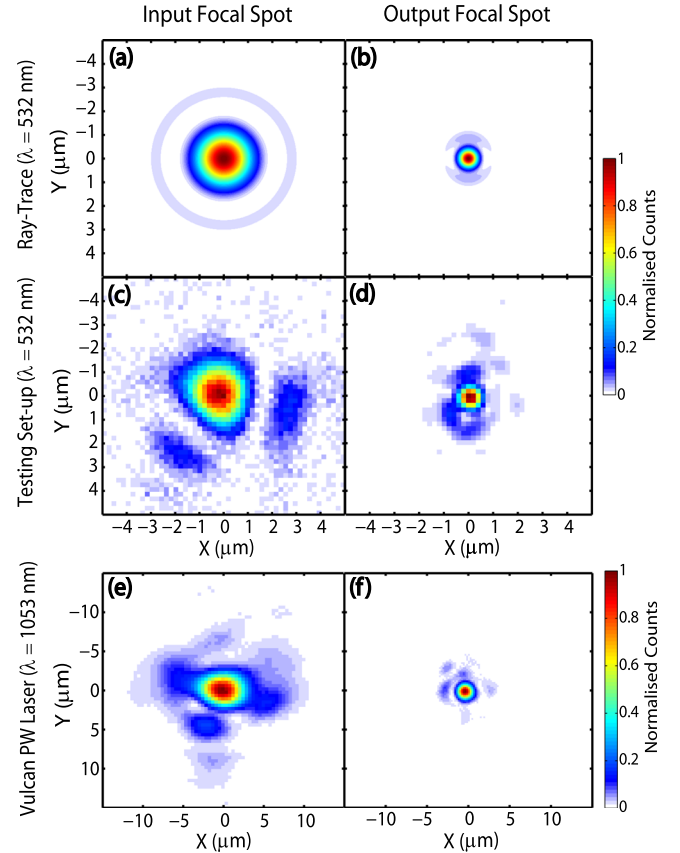


FIG. 3. (a) and (b) Calculated laser focal spot distributions at (a) f_1 and (b) f_2 from Zemax ray trace modelling of the FPM operation. (c) and (d) Corresponding measured spatial-intensity distributions using the characterisation set-up (with 532 nm light). (e) and (f) Corresponding measured focal spot distributions using the Vulcan PW laser, with low power (CW operation) 1053 nm light.

central wavelength of 1053 nm. A factor of $\times 2.5$ reduction in the spot FWHM (from $4.0 \mu\text{m}$ input to $1.6 \mu\text{m}$ output) and an increase in the FWHM encircled energy from 28.1% to 36.5% are found. This FWHM encircled energy value for the output focal spot is a factor of 2.2 increase over earlier proof-of-principle experiments.²⁶ The test results with the Vulcan PW laser are seen to be in good agreement with the earlier tests using 532 nm light shown in Figs. 3(c) and 3(d). These results indicate that a peak intensity of $3.4 \times 10^{21} \text{ W cm}^{-2}$ could be achieved using the Vulcan PW laser parameters giving a factor of ~ 5.3 intensity enhancement over the standard OAP focusing.

Sensitivity to misalignment

Successful FPM operation depends strongly upon achieving optimised alignment, as presented in Fig. 3, which is reliant upon the OAP focus spatially coinciding with f_1 , thus accurate optic positioning. Exploring the effect of misalignment is important to test the feasibility of these optics. Variations in the OAP focus position can occur on the micron scale on high power laser systems due to various effects, including thermal lensing in the laser chain which can alter the divergence of the incoming pulse prior to focusing. The testing set-up was used to implement a controlled displacement in the OAP focus position, relative to f_1 , for

the three possible displacement directions, Δx , Δy , and Δz . Figures 4(a) and 4(b) shows the effect on the output focus quality for varying degrees of misalignment. This is quantified by measuring the percentage of focal spot energy contained within a circle of diameter equal to the FWHM of the optimised focus (Fig. 3(d)).

It is evident from Fig. 4(a) that displacements in Δx and Δy result in the quality of the output focus being degraded. Results indicate that intensity enhancement with the FPM can only be achieved for displacements of $<10\ \mu\text{m}$, for misalignments in only one axis (Δx or Δy). Above this value, and in misalignments of both axis simultaneously (Δxy), the focal spot quality is sufficiently degraded that no intensity enhancement is achievable.

Figure 4(b) shows the effect of a longitudinal OAP displacement, Δz . A displacement of this type results in the output image position, nominally at f_2 , being displaced to a new effective best position. Accordingly this misalignment can

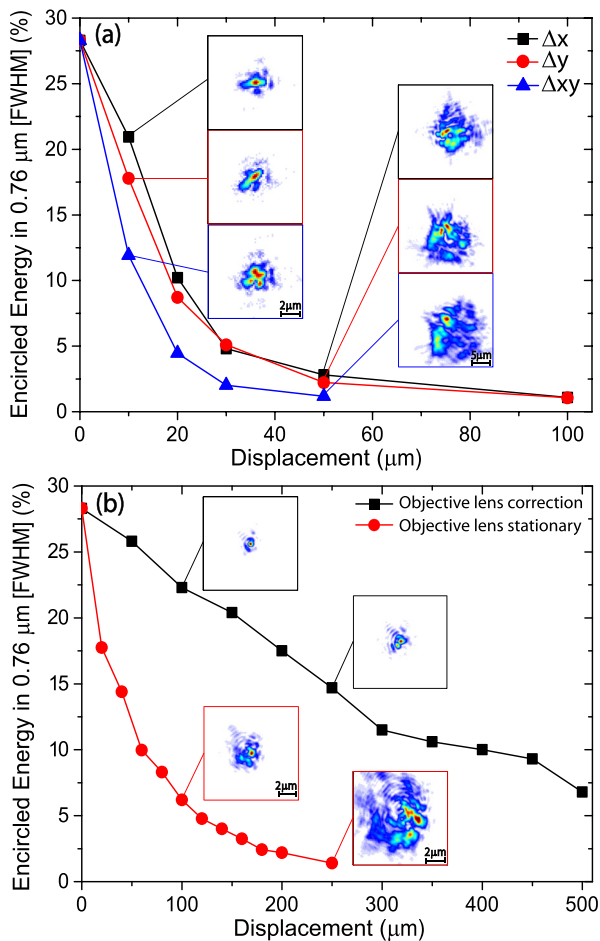


FIG. 4. (a) Plot of the output focus (f_2) encircled energy percentage contained within a circle of diameter equal to the FWHM optimised focal spot (i.e., $0.76\ \mu\text{m}$), as a function of OAP focus displacements from position f_1 . Black symbols correspond to Δx ; red symbols correspond to Δy ; and blue symbols correspond to Δxy (equal magnitude in x and y) displacements. (b) Same, but for the case where the OAP displacement is along the input beam direction, Δz . Black symbols correspond to the case where the objective lens image plane is adjusted to locate the best focus, i.e., maximised encircled energy, and red symbols correspond to the case where it remains stationary at the position of optimised alignment focus, i.e., f_2 . In both (a) and (b) the insets are images of the effect on output focus due to the various misalignments.

be characterised in two ways: (1) with the objective lens translated to account for the OAP displacements and (2) with the objective lens fixed at position f_2 . The latter case is analogous to an interaction target placed at the nominal focus position and is thus important for practical use of the optic.

When the objective lens is translated, Fig. 4(b) (black data points), the output focal spot quality remains relatively high compared to the other misalignment forms, i.e., Δx and Δy , over a larger range of displacement. Intensity enhancement is achieved over a $\pm 300\ \mu\text{m}$ range either side of the optimum alignment position. Characterisation of this misalignment and the Δx , Δy , and Δxy cases are highly beneficial as the degree and direction of energy spread present relate to the direction and magnitude of the misalignment, which consequently helps to optimise the FPM alignment. In the second case, when the objective lens remains fixed at position f_2 , Fig. 4(b) (red data points), intensity enhancement is only possible for displacements of $<30\ \mu\text{m}$, due to fast degradation of the focal spot quality with increased misalignment.

To quantify the magnitude of the longitudinal displacements in the OAP focus position from nominal (which the FPM is aligned to) which may occur on the Vulcan PW laser, a Shack-Hartmann wavefront sensor was employed to measure the degree of phase aberrations present in the laser wavefront; aberrations which will result in non-ideal focusing from the OAP. This measurement is critical to gauge if the use of an FPM is beneficial in terms of intensity enhancement or if shot-to-shot misalignments are too large to achieve enhancement. Fluctuations in the OAP focus position were measured over a series of full energy shots, with average values $<20\ \mu\text{m}$ observed. The resultant displacement from position f_2 to the effective best focus, Δv , as a function of this shift, Δu , is found to be equal $\Delta v = -m^2 \Delta u$ (m being the FPM magnification [$m = 1/3$]). This is confirmed both experimentally and by the ray-trace model. A value $\Delta u = 20\ \mu\text{m}$ would therefore yield a $2.2\ \mu\text{m}$ displacement in the output focus position. The consequence of this is that a target aligned to the nominal focus would be irradiated with a pulse with a factor $\times 2.3$ peak intensity reduction (from 3.4×10^{21} to $1.5 \times 10^{21}\ \text{W cm}^{-2}$). This would still result in an intensity enhancement over the direct target irradiation with the F/3.1 OAP. This analysis demonstrates the importance of monitoring the degree of OAP focus position displacement when using an FPM in order to assess its operation and assess the level of intensity enhancement achieved.

Optic testing in plasma operation

The final test of the FPM was to investigate its operation under plasma conditions using the Vulcan PW laser and quantify the effect of displacement of the input focus. Figure 1 shows an overview of the optical set-up for both the FPM and PPM. As the focal spot formed by the optic cannot be directly measured during a full power laser shot (i.e., when used in plasma operation), the success of the FPM in enhancing the focused intensity was diagnosed via measurements of the maximum energy of protons accelerated from foil targets positioned at f_2 (as in the previous demonstration experiments^{25,26}). The laser-plasma acceleration mechanism utilised

is known as target normal sheath acceleration (TNSA).³¹ This results from a strong electrostatic field formed at the target rear surface, by fast electrons produced at the front side and transported through the foil. The maximum proton energy achieved via this mechanism is correlated to the peak laser intensity,^{32,33} via the temperature and density of the fast electrons.³⁴

Proton acceleration was achieved using either a FPM or a PPM, both made from the same material (PMMA). The PPM shots were necessary to acquire reference proton energies with the same reflectivity and intensity contrast enhancement to gauge the FPM performance. p-polarised pulses incident at 0° to aluminium target foils with thickness equal to $6\ \mu\text{m}$ and transverse dimensions $1\text{ mm} \times 1\text{ mm}$ were used throughout. Accelerated protons were detected using a stack of dosimetry (radiochromic, RCF)³⁵ film positioned 50 mm behind the target foil centred on the target normal axis. This enables proton energy measurements to be made at discrete energies. Figures 5(a) and 5(b) summarise the results of a series of shots using both plasma mirror types.

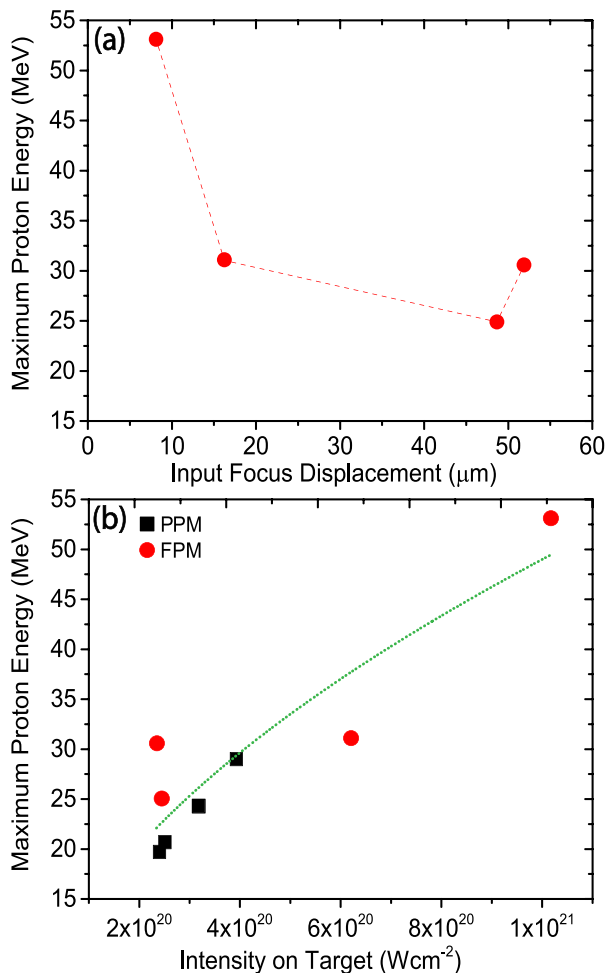


FIG. 5. (a) Plot of the measured maximum proton energy, achieved using the FPM, as a function of the longitudinal displacement measured in the input focal spot position from f_1 . (b) Plot of the measured maximum proton energy (E_{pmax}) achieved with both the FPM (red circles) and PPM (black squares), as a function of the intensity (I) on target, when taking into account the displacement in OAP focus position. In the PPM cases, intensity was varied by changing the pulse energy. The dotted line represents a simple power fit (of the form $E_{pmax} = a.I^b$) to show the approximate scaling of the maximum proton energy with peak laser intensity.

A maximum proton energy in the range 24.9–53.1 MeV was measured when using the FPMs, and 19.7–29.0 MeV was measured for the PPM shots. Comparing the maximum of these ranges, almost a factor of 2 enhancement was achieved by employing the FPM. This increase occurs with an estimated intensity enhancement factor of $\times 2.6$ (from $3.9 \times 10^{20}\text{ W cm}^{-2}$ to $1.0 \times 10^{21}\text{ W cm}^{-2}$). It should be noted that the intensity achieved using the FPM is lower than predicted from the characterisation study, Figs. 3(e) and 3(f) ($3.4 \times 10^{21}\text{ W cm}^{-2}$), due to a lower on-target pulse energy than that used to calculate the predicted value, caused by a lower than expected energy throughput from compressor.

Not all of the FPM shots resulted in higher proton energies. This is due to a non-optimum alignment caused by a longitudinal shift in the input focus position, as characterised in Fig. 4(b). On each FPM shot, the wavefront quality of the pulses was measured to gauge the magnitude of misalignment that the optic is subject to. The changes in the output focal spot size and encircled energy are used in the calculation of the resultant intensity on target. The FPM shot which achieved the highest proton energy (53.1 MeV) was determined to be close to the optimum alignment, compared to the other shots which yielded lower proton energies, as shown in Fig. 5(a). Figure 5(b) shows the calculated peak intensity when taking this misalignment into consideration. It is clear that the reduced proton maximum energy on some FPM shots occurred due to the peak intensity being reduced to a similar level as that achieved with the PPM shots. A simple power scaling fit to the complete data set, of the form $E_{pmax} = a.I^b$, results in $b = 0.55 \pm 0.1$. This is in good agreement with the TNSA proton energy scaling reported in Refs. 32 and 33, in which the maximum proton energy is found to be proportional to the fast-electron temperature, which scales with the ponderomotive potential ($\propto (I\lambda^2)^{1/2}$, where I is the laser intensity and λ is the laser wavelength).³⁶ We note however that even when correcting for the reduction in intensity due to misalignment of the OAP focus with respect to the f_1 position, the FPM data does not follow the TNSA scaling fit as strongly as the PPM data. This may point to other sources of error affecting the peak intensity achieved—for example, in accurately positioning of the target at the focus (f_2) of the small F/# beam due to the very small Rayleigh range ($\sim 5.5\ \mu\text{m}$). This issue will be investigated in more detail in future work.

These test results indicate that the FPM does successfully enhance the intensity when optimally aligned, as indicated by the factor of 2 increase in maximum proton energy, but that successful operation crucially depends on minimising the displacement of the input focus with respect to position f_1 .

SUMMARY

The design, testing, and demonstration of a focusing plasma mirror, based on an ellipsoidal geometry for demagnification of an ultra-intense laser focal spot, are reported. The design involved optimisation of the incident laser intensity to maximise the plasma reflectivity. The reflected energy on full power shots with the FPM is found to be $\sim 15\%$ – 20%

lower than the value predicted in the design (as shown in Fig. 2). This difference will be investigated in detail in future work, together with the effect of adding an AR coating to increase the plasma mirror intensity contrast enhancement factor, enabling investigations utilising sub-micron solid targets.

Direct measurements of the focal spot formed by the FPM using a low-energy laser demonstrated a factor of $\times 2.5$ reduction in focal spot size, resulting in an estimated factor of $\times 3.6$ intensity enhancement, when considering the focal spot quality (encircled energy) and the reflectivity. It is found that the optics focal spot quantity is very sensitive to misalignments, but when minimised successful FPM operation is achieved. This is demonstrated through the enhancement of maximum proton energies accelerated from foil targets when the optic is optimally aligned.

An example use of the FPM in an investigation of laser-driven proton acceleration is demonstrated. The highest proton energies are achieved when the optic is aligned within $10\text{ }\mu\text{m}$ of the optimum position. Larger misalignment results in lower proton energy, such that the benefit of the FPM over a PPM is lost.

Due to the limited research performed to date on this type of focusing plasma optic, especially in conjunction with petawatt scale laser systems, the present study helps to bring plasma-based optical technology closer to maturity. Under optimum alignment conditions, a peak intensity of $\sim 4 \times 10^{21}\text{ W cm}^{-2}$ could be achieved when employing the FPM on the Vulcan PW laser system, as determined from the focal spot characterisation. Optimisation of the Vulcan laser to enhance the pulse energy and to decrease the pulse duration could yield peak intensities close to 10^{22} W cm^{-2} when using the FPM. This would provide a window into the physics achievable with future multi-petawatt laser systems. Focusing plasma mirrors such as the type described here could also be developed for use on these higher power lasers, which would also push the intensity frontier achievable yet further. During the process, this will open up the exploration of new high field physics phenomena at the focus of intense laser pulses.

ACKNOWLEDGMENTS

We acknowledge the expert support of staff at the Central Laser Facility of the Rutherford Appleton Laboratory. This research was financially supported by EPSRC (Grant Nos. EP/J003832/1, EP/L001357/1, and EP/K022415/1). Data associated with the research published in this paper can be accessed at: <http://dx.doi.org/10.15129/e778dc67-2b5e-40b5-b701-adb1caefee19>.

¹A. Macchi, M. Borghesi, and M. Passoni, *Rev. Mod. Phys.* **85**, 751–793 (2013).

²E. Esarey, C. B. Schroeder, and W. P. Leemans, *Rev. Mod. Phys.* **81**, 1229 (2009).

³P. A. Norreys, M. Santala, E. Clark, M. Zepf, I. Watts, F. N. Beg, K. Krushelnick, M. Tatarakis, A. E. Dangor, X. Fang, P. Graham, T. McCanny, R. P. Singhal, K. W. D. Ledingham, A. Creswell, D. C. W. Sanderson, J. Magill, A. Machacek, J. S. Wark, R. Allott, B. Kennedy, and D. Neely, *Phys. Plasmas* **6**, 2150 (1999).

⁴S. Cipiccia, M. R. Islam, B. Ersfeld, R. P. Shanks, E. Brunetti, G. Vieux, X. Yang, R. C. Issac, S. M. Wiggins, G. H. Welsh, M. Anania, D. Maneuski, R. Montgomery, G. Smith, M. Hoek, D. J. Hamilton, N. R. C.

Lemos, D. Symes, P. P. Rajeev, V. O. Shea, J. M. Dias, and D. A. Jaroszynski, *Nat. Phys.* **7**, 867–871 (2011).

⁵J. H. Bin, W. J. Ma, H. Y. Wang, M. J. V. Streeter, C. Kreuzer, D. Kiefer, M. Yeung, S. Cousens, P. S. Foster, B. Dromey, X. Q. Yan, R. Ramis, J. Meyer-ter-Vehn, M. Zepf, and J. Schreiber, *Phys. Rev. Lett.* **115**, 064801 (2015).

⁶B. Gonzalez-Izquierdo, R. J. Gray, M. King, R. J. Dance, R. Wilson, J. McCreadie, N. M. H. Butler, R. Capdessus, S. Hawkes, J. S. Green, M. Borghesi, D. Neely, and P. McKenna, *Nat. Phys.* (published online).

⁷G. Gregori, A. Ravasio, C. D. Murphy, K. Schaar, A. Baird, A. R. Bell, A. Benuzzi-Mounaix, R. Bingham, C. Constantin, R. P. Drake, M. Edwards, E. T. Everson, C. D. Gregory, Y. Kuramitsu, W. Lau, J. Mithen, C. Niemann, H.-S. Park, B. A. Remington, B. Reville, A. P. L. Robinson, D. D. Ryutov, Y. Sakawa, S. Yang, N. C. Woolsey, M. Koenig, and F. Miniati, *Nature* **481**, 480–483 (2012).

⁸C. D. Gregory, J. Howe, B. Loupias, S. Myers, M. M. Notley, Y. Sakawa, A. Oya, R. Kodama, M. Koenig, and N. C. Woolsey, *Astrophys. J.* **676**, 420–426 (2008).

⁹A. Benuzzi-Mounaix, S. Mazevet, A. Ravasio, T. Vinci, A. Denoeud, M. Koenig, N. Amadou, E. Brambrink, F. Festa, A. Levy, M. Harmand, S. Brygoo, G. Huser, V. Recoules, J. Bouchet, G. Morard, F. Guyot, T. de Resseguier, K. Myanishi, N. Ozaki, F. Dorchies, J. Gaudin, P. Marie Leguay, O. Peyrusse, O. Henry, D. Raffestin, S. Le Pape, R. Smith, and R. Musella, *Phys. Scr.* **T161**, 014060 (2014).

¹⁰D. A. MacLellan, D. C. Carroll, R. J. Gray, A. P. L. Robinson, M. P. Desjarlais, D. Neely, and P. McKenna, *Plasma Phys. Controlled Fusion* **56**, 084002 (2014).

¹¹J. P. Zou, C. Le Blanc, D. N. Papadopoulos, G. Chériaux, P. Georges, G. Mennerat, F. Druon, L. Lecherbourg, A. Pellegrina, P. Ramirez, F. Giambruno, A. Frénaux, F. Leconte, D. Badarau, J. M. Boudenne, D. Fournet, T. Valloton, J. L. Paillard, J. L. Veray, M. Pina, P. Monot, J. P. Chambaret, P. Martin, F. Mathieu, P. Audebert, and F. Amiranof, *High Power Laser Sci. Eng.* **3**, e2 (2015).

¹²B. Rus, P. Bakule, D. Kramer, G. Korn, J. T. Green, J. Novák, M. Fibrich, F. Batysta, J. Thoma, J. Naylor, T. Mazanec, M. Vitek, R. Barros, E. Koutiris, J. Hřebíček, J. Polan, R. Baše, P. Homer, M. Košelja, T. Havlíček, A. Honsa, M. Novák, C. Zervos, P. Korous, M. Laub, and J. Houzvička, “High-power, high-energy, and high-intensity laser technology; and research using extreme light: Entering new frontiers with petawatt-class lasers,” *Proc. SPIE* **8780**, 87801T (2013).

¹³C. P. Ridgers, C. S. Brady, R. Ducloux, J. G. Kirk, K. Bennett, T. D. Arber, and A. R. Bell, *Phys. Plasmas* **20**, 056701 (2013).

¹⁴R. Capdessus and P. McKenna, *Phys. Rev. E* **91**, 053105 (2015).

¹⁵G. Doumy, F. Quéré, O. Gobert, M. Perdrix, Ph. Martin, P. Audebert, J. C. Gauthier, J.-P. Geindre, and T. Wittmann, *Phys. Rev. E* **69**, 026402 (2004).

¹⁶D. Neely, P. Foster, A. Robinson, F. Lindau, O. Lundh, A. Persson, C.-G. Wahlström, and P. McKenna, *Appl. Phys. Lett.* **89**, 021502 (2006).

¹⁷D. Strickland and G. Mourou, *Opt. Commun.* **55**, 447–449 (1985).

¹⁸H. W. Powell, M. King, R. J. Gray, D. A. MacLellan, B. Gonzalez-Izquierdo, L. C. Stockhausen, G. Hicks, N. P. Dover, D. R. Rusby, D. C. Carroll, H. Padda, R. Torres, S. Kar, R. J. Clarke, I. O. Musgrave, Z. Najmudin, M. Borghesi, D. Neely, and P. McKenna, *New J. Phys.* **17**, 103033 (2015).

¹⁹B. Dromey, M. Zepf, A. Gopal, K. Lancaster, M. S. Wei, K. Krushelnick, M. Tatarakis, N. Vakis, S. Moustazis, R. Kodama, M. Tampo, C. Stoeckl, R. Clarke, H. Habara, D. Neely, S. Karsch, and P. Norreys, *Nat. Phys.* **2**, 456–459 (2006).

²⁰C. Thauray and F. Quéré, *J. Phys. B: At., Mol. Opt. Phys.* **43**, 213001 (2010).

²¹Ch. Ziener, P. S. Foster, E. J. Divall, C. J. Hooker, M. H. R. Hutchinson, A. J. Langley, and D. Neely, *J. Appl. Phys.* **93**, 768 (2003).

²²B. Dromey, S. Kar, M. Zepf, and P. Foster, *Rev. Sci. Instrum.* **75**, 645 (2004).

²³T. Wittmann, J. P. Geindre, P. Audebert, R. S. Marjoribanks, J. P. Rousseau, F. Burgu, D. Douillet, T. Lefrou, K. Ta Phuoc, and J. P. Chambaret, *Rev. Sci. Instrum.* **77**, 083109 (2006).

²⁴G. G. Scott, V. Bagnoud, C. Brabetz, R. J. Clarke, J. S. Green, R. I. Heathcote, H. W. Powell, B. Zielbauer, T. D. Arber, P. McKenna, and D. Neely, *New J. Phys.* **17**, 033027 (2015).

²⁵A. Kon, M. Nakatsutsumi, S. Buffechoux, Z. L. Chen, J. Fuchs, Z. Jin, and R. Kodama, *J. Phys.: Conf. Ser.* **244**, 032008 (2010).

- ²⁶M. Nakatsutsumi, A. Kon, S. Buffechoux, P. Audebert, J. Fuchs, and R. Kodama, *Opt. Lett.* **35**, 2314–2316 (2010).
- ²⁷O. N. Stavroudis and A. J. Ames, *J. Opt. Soc. Am. A* **9**, 2083–2088 (1992).
- ²⁸P. Monot, G. Doumy, S. Dobosz, M. Perdrix, P. D'Oliveira, F. Quéré, F. Réau, P. Martin, P. Audebert, J.-C. Gauthier, and J.-P. Geindre, *Opt. Lett.* **29**, 893–895 (2004).
- ²⁹C. Thauray, F. Quéré, J.-P. Geindre, A. Levy, T. Ceccotti, P. Monot, M. Bougeard, F. Réau, P. d'Oliveira, P. Audebert, R. Marjoribanks, and Ph. Martin, *Nat. Phys.* **3**, 424–429 (2007).
- ³⁰Y. Nomura, L. Veisz, K. Schmid, T. Wittmann, J. Wild, and F. Krausz, *New J. Phys.* **9**, 9 (2007).
- ³¹S. C. Wilks, A. B. Langdon, T. E. Cowan, M. Roth, M. Singh, S. Hatchett, M. H. Key, D. Pennington, A. MacKinnon, and R. A. Snavely, *Phys. Plasmas* **8**, 542 (2001).
- ³²L. Robson, P. T. Simpson, R. J. Clarke, K. W. D. Ledingham, F. Lindau, O. Lundh, T. McCanny, P. Mora, D. Neely, C.-G. Wahlström, M. Zepf, and P. McKenna, *Nat. Phys.* **3**, 58–62 (2007).
- ³³J. Fuchs, P. Antici, E. d'Humières, E. Lefebvre, M. Borghesi, E. Brambrink, C. A. Cecchetti, M. Kaluza, V. Malka, M. Manclossi, S. Meyroneinc, P. Mora, J. Schreiber, T. Toncian, H. Pépin, and P. Audebert, *Nat. Phys.* **2**, 48–54 (2006).
- ³⁴P. Mora, *Phys. Rev. Lett.* **90**, 185002 (2003).
- ³⁵F. Nürnberg, M. Schollmeier, E. Brambrink, A. Blažević, D. C. Carroll, K. Flippo, D. C. Gautier, M. Geißel, K. Harres, B. M. Hegelich, O. Lundh, K. Markey, P. McKenna, D. Neely, J. Schreiber, and M. Roth, *Rev. Sci. Instrum.* **80**, 033301 (2009).
- ³⁶S. C. Wilks, W. L. Kruer, M. Tabak, and A. B. Langdon, *Phys. Rev. Lett.* **69**, 1383 (1992).